Electronic Supplementary Material (ESI) for Chemical Communications.

Halogen bonding in UiO-66 Frameworks Promotes Superior Chemical Warfare Agent Simulant Degradation

Mark Kalaj, Mohammad R. Momeni, Kyle C. Bentz, Kyle S. Barcus, Joseph M. Palomba, Francesco Paesani, and Seth M. Cohen*

Department of Chemistry and Biochemistry, University of California, San Diego, La Jolla, California 92093, United States

Materials Synthesis

All solvents and starting materials were purchased from chemical suppliers and used without further purification (Sigma Aldrich, Alfa Aesar, EMD, and TCI).

Ligand Syntheses

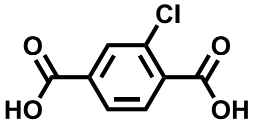

2-Chloroterephthalic acid. 2-Chloro-1,4-dimethylbenzene (6 mL, 43 mmol), 60 mL of deionized water and 16 ml of nitric acid (70%) were poured into a 100 ml Teflon-lined steel autoclave. The autoclave was sealed and placed into a 170 °C oven for 16 h. After cooling to room temperature, the solution was vacuum filtered and 2-chloroterephthalic acid was recovered as a white crystalline powder which was washed with water and dried in a vacuum oven at 70 °C overnight. Yield: 5.4 g (63%). ^{1}H NMR (400 MHz, d_6-DMSO): δ 13.65 (s, 2H), 7.98 (d, J = 1.2 Hz, 1H), 7.95 (dd, J = 8.0, 1.5 Hz, 1H), 7.87 (d, J = 8.0 Hz, 1H). MS (m/z) calcd. for $C_8H_5ClO_4$ [M-H]$^-$: 198.99; Found: 199.07.

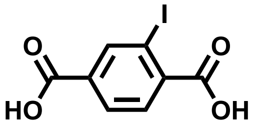

2-Iodoterephthalic acid. To a suspension of 2-aminoterephthalic acid (3.0 g, 16.6 mmol) in 100 mL of H_2O/ conc. HCl (1:1, v/v) at 0 °C, an aqueous solution of $NaNO_2$ (2.85 g, 41.3 mmol) was added dropwise over a period of 45 min. After being stirred for an additional 30 min at 0 °C, the diazonium salt was poured into a solution of KI (16.5 g, 99.4 mmol) in 150 mL of water and the resulting dark solution was left stirring at room temperature for 18 h. Solid $NaHSO_3$ was added in portions until the dark color of the solution faded, leaving a behind a suspension of tan colored solid in the solvent mixture. The solid was filtered and triturated with 150 mL of CH_2Cl_2:H_2O (1:1, v/v) and dried overnight in a vacuum oven. Yield: 4.03 g (83%). ^1H NMR (400 MHz d_6-DMSO): δ 13.57 (s, 2H), 8.42 (d, $J = 1.4$ Hz, 1H), 7.99 (dd, $J = 8.0$, 1.6 Hz, 1H), 7.77 (d, $J = 8.0$ Hz, 1H). MS (m/z) calcd. for $C_8H_5IO_4$ $[M-H]^-$: 290.92; Found: 290.97.

MOF Syntheses

UiO-66. Zirconium(IV) chloride (61 mg, 0.26 mmol) and terephthalic acid (43 mg, 0.26 mmol) were dissolved in 15 mL DMF with 0.45 mL glacial acetic acid in a 20 mL vial with Teflon-lined cap. The vial was then placed in a 120 °C oven for 24 h. After cooling to ambient temperature, the particles were collected by centrifugation (fixed-angle rotor, 6000 rpm, 5 min), followed by washing with 3×10 mL DMF and 3×10 mL MeOH. The particles were then soaked in MeOH for 3 d with solvent changed daily, before being dried under vacuum at room temperature.

UiO-66-F. Zirconium(IV) chloride (61 mg, 0.26 mmol) and 2-fluoroterephthalic acid (48 mg, 0.26 mmol) were dissolved in 15 mL DMF with 0.45 mL glacial acetic acid in a 20mL vial with Teflon-lined cap. The vial was then placed in a 120 °C oven for 24 h. After cooling to ambient temperature, the particles were collected by centrifugation (fixed-angle rotor, 6000 rpm, 5 min), followed by washing with 3×10 mL DMF and 3×10 mL MeOH. The particles were then soaked in MeOH for 3 d with solvent changed daily, before being dried under vacuum at room temperature.

UiO-66-Cl. Zirconium(IV) chloride (61 mg, 0.26 mmol) and 2-chloroterephthalic acid (52 mg, 0.26 mmol) were dissolved in 15 mL DMF with 0.45 mL glacial acetic acid in a 20 mL vial with Teflon-lined cap. The vial was then placed in a 120 °C oven for 24 h. After cooling to ambient temperature, the particles were collected by centrifugation (fixed-angle rotor, 6000 rpm, 5 min), followed by washing with 3×10 mL DMF and 3×10 mL MeOH. The particles were then soaked in MeOH for 3 d with solvent changed daily, before being dried under vacuum at room temperature.

UiO-66-Br. Zirconium(IV) chloride (61 mg, 0.26 mmol) and 2-bromoterephthalic acid (64 mg, 0.26 mmol) were dissolved in 15 mL DMF with 0.45 mL glacial acetic acid in a 20mL vial with Teflon-lined cap. The vial was then placed in a 120 °C oven for 24 h. After cooling to ambient temperature, the particles were collected by centrifugation (fixed-angle rotor, 6000 rpm, 5 min), followed by washing with 3×10 mL DMF and 3×10 mL MeOH. The particles were then soaked in MeOH for 3 d with solvent changed daily, before being dried under vacuum at room temperature.

UiO-66-I. Zirconium(IV) chloride (61 mg, 0.26 mmol) and 2-iodoterephthalic acid (76 mg, 0.26 mmol) were dissolved in 15 mL DMF with 0.45 mL glacial acetic acid in a 20 mL vial with Teflon-lined cap. The vial was then placed in a 120 °C oven for 24 h. After cooling to ambient temperature, the particles were collected by centrifugation (fixed-angle rotor, 6000 rpm, 5 min), followed by washing with 3×10 mL DMF and 3×10 mL MeOH. The particles were then soaked in MeOH for 3 d with solvent changed daily, before being dried under vacuum at room temperature.

UiO-66-I$_{50\%}$ Zirconium (IV) chloride (61 mg, 0.26 mmol), 2-iodoterephthalic acid (38 mg, 0.13 mmol) and terephthalic acid (22 mg, 0.13 mmol) were dissolved in 15 mL DMF with 0.45 mL glacial acetic acid in a 20mL vial with Teflon-lined cap. The vial was then placed in a 120 °C oven for 24 h. After cooling to ambient temperature, the particles were collected by centrifugation (fixed-angle rotor, 6000 rpm, 5 min), followed by washing with 3×10 mL DMF and 3×10 mL MeOH. The particles were then soaked in MeOH for 3 d with solvent changed daily, before being dried under vacuum at room temperature.

Characterization Methods

Powder X-ray Diffraction (PXRD). PXRD data was collected at room temperature on a Bruker D8 Advance diffractometer running at 40 kV, 40 mA for Cu Kα ($\lambda = 1.5418$ Å), with a scan speed of 0.5 sec/step, a step size of 0.01° in 2θ, and a 2θ range of 3-50° at room temperature.

Scanning Electron Microscopy (SEM). MOFs were placed on conductive carbon tape on a sample holder and coated using an Ir-sputter coating for 7 sec. A Zeiss Sigma 500 ESEM microscope was used for acquiring images using a 2-3 kV energy source under vacuum at a working distance of 5 mm.

Thermogravimetric analysis and differential scanning calorimetry (TGA/DSC). ~10 mg of sample was placed in a 100 μL aluminum crucible. Samples were analyzed on a

Mettler Toledo Star TGA/DSC using a temperature range of 30-600 °C scanning at 10 °C/min under a synthetic air atmosphere (75 cm^3/min air flow rate) for sample degradation measurements.

Nuclear Magnetic Resonance. Proton nuclear magnetic resonance spectra (^{1}H NMR) were recorded on a Varian FT-NMR spectrometer (400 MHz). Chemical shifts are quoted in parts per million (ppm) referenced to the appropriate solvent peak or 0 ppm for TMS. MOFs were digested for NMR analysis by immersion of ~8-10 mg MOF in 580 μL DMSO-d_6 with 20 μL HF (48% in water). Samples were kept in this acidic solution at room temperature until the MOF was fully dissolved.

N_2 Gas Sorption Analysis: Samples for analysis were evacuated in a vacuum oven overnight at room temperature prior to analysis. ~50 mg of sample was then transferred to pre-weighed sample tubes and degassed at 105 °C on a Micromeritics ASAP 2020 Adsorption Analyzer for a minimum of 12 h or until the outgas rate was <5 mmHG. After degassing, the sample tubes were re-weighed to obtain a consistent mass for the samples. Sorption data and BET surface area (m^2/g) measurements were collected at 77 K with N_2 on a Micromeritics ASAP 2020 Adsorption Analyzer using volumetric technique.

Catalysis Experiments. In this study, DMNP hydrolysis was measured using a modified version of a previously reported procedure (*Chem. Commun.* **2018**, *54*, 5768-5771). All catalytic monitoring was carried out using a BioTek Synergy H4 plate reader using single wavelength absorbance mode. 20 and 40 mM of *N*-ethylmorpholine buffer was prepared from deionized water adjusted to pH = 8.0. A plot of absorbance of *p*-nitrophenol at varying concentrations was measured yielding a calibration curve with a slope of 3.48 Abs/mM (*Chem. Commun.* **2018**, *54*, 5768-5771). MOF samples were prepared by weighing 6 mg of MOF powder and diluting this powder in 10 mL of deionized water. These solutions were rigorously sonicated and vortexed (>3× of each) and diluted in half with 40 mM buffer solution yielding 300 μg/mL MOF in 20 mM buffer solution. Dimethyl *p*-nitrophenylphosphate (DMNP) hydrolysis assays with MOF powders were carried out in Olympus Plastics clear, flat-bottom 96-well plates. Each well was prepared with 100 μL total volume containing: 95 μL MOF suspension in buffer and 5 μL substrate (25 mM DMNP in MeOH; 1.25 mM total concentration; 0.125 μmol). Upon the addition of substrate using a multi-channel pipette, hydrolysis was monitored by the change in absorbance (λ_{max} = 407 nm) over 15 min at 24 °C with 3 sec shaking of the plate every 10 sec. The absorbance was monitored from the 30 to 360 sec time period, instead of the previously reported 600 to 3000 sec time period (*Chem. Commun.* **2018**, *54*, 5768-5771). This adjustment was made because raw data of our most active sample, UiO-66-I, displays a drastic difference in slope after ~500 sec in the absorbance vs. time curve (Figure S24). When the data is analyzed in the 30 to 360 sec regions, the slope of the line is consistent throughout. As such, in an attempt to obtain a more accurate value of the rate of catalysis, data from 30 sec to 360 sec was used to calculate the hydrolysis of DMNP (Figure S24) for all samples. Activity was measured as initial linear rate, measured from 30 to 360 sec using Excel software. Reported activities for MOF samples are an average of seven replicates. Hydrolysis rates were adjusted to account for the increased mass of the halogenated species such that a direct comparison could be made across all materials in this study (Figure S25). Rates were calculated to account for the substantial difference in moles of MOF catalyst between samples (due to the increased mass of the halogenated MOFs) such that a direct comparison could be made across all materials in this study. For example, a single SBU of UiO-66 has a molecular mass of 1628 g/mol, whereas a single SBU of UiO-66-I has a molecular mass of 2383 g/mol. The difference in number of moles per sample well was account for as shown in Table S1.

Table S1. Corrected hydrolysis calculation to account for increased mass of halogenated materials.

MOF	**Molar Mass of MOF (*g/mol*)**	**Mole ratio to UiO-66 Standard**	**Expermental Hydrolysis Rate**[a] **(*k*, mM/sec)**	**Molar Mass Corrected Hydrolysis Rate (*k*, mM/sec)**
NU-1000	1624	1.00	133	133
UiO-66	1628	1.00	161	161
UiO-66-F	1736	0.94	213	226
UiO-66-Cl	1835	0.89	172	194
UiO-66-Br	2101	0.77	134	173
UiO-66-I$_{50\%}$	2016	0.81	337	417
UiO-66-I	2383	0.68	413	605

[a] 6 mg of MOF used in each experiment.

Computational Details

Periodic Calculations. PBE (Perdew et al., *Phys. Rev. Lett.* **1996,** *77,* 3865-3868) density functional calculations with damped D3 dispersion correction (Grimme et al., *J. Comp. Chem.* **2006**, *27*, 1787-1799) as implemented in CP2K version 5.1 (Hutter et al., *Wiley Interdisciplinary Rev. Comput. Mol. Sci.* **2014**, *4*, 15-25) were performed to fully relax both atomic positions and cell parameters of the pristine (12 BDC linkers, 456 atoms) and mono-defective (11 BDC linkers, 450 atoms) UiO-66 MOFs (Figure S26). For the latter, the two open Zr^{IV} metal-sites resulted after one BDC removal were saturated and charge balanced by adding two water and two hydroxyl groups (Planas et al., *J. Phys. Chem. Lett.* **2014,** *5,* 3716-3723).

The double-zeta valence with polarization DZVP-MOLOPT basis sets and core electron pseudopotentials according to the Geodecker−Teter−Hutter formulation (Goedecker et al. *Phys. Rev. B* **1996,** *54, 1703-1710)* were used. The plane-wave cutoff of the finest grid and REL_CUTOFF were set to 360 RY and 60 RY. MAX_FORCE (hartree/bohr), RMS_FORCE, MAX_DR (bohr), and RMS_DR were set to 0.0030, 0.0050, 0.0020, and 0.0050, respectively. Vibrational frequency calculations were performed numerically at the Γ point on a fragment comprised of the metal−oxide node (without the linkers) to assure presence of a local minimum on the potential energy surface.

Cluster Calculations. Cluster models were cut from the optimized periodic conventional unit cell of the mono-defective UiO-66. To obtain these cluster models, the organic linkers around the metal−oxide node were truncated to four benzoate linkers on top face, which are toward DMNP, with the 8 remaining linkers truncated to formate (Figure S27, Cartesian coordinates of all optimized structures are included as part of the Supporting Information (SI)).

The carbon atoms of all the carboxylate linkers were fixed to keep the rigidity of the MOF. The meta-GGA local M06-L (Zhao et al., *J. Chem. Phys.* **2006**, *125*, 194101) density functional was used for all geometry optimizations in gas phase using the Def2-SVP (Weigend et al., *Phys. Chem. Chem. Phys.* **2006**, *8*, 1057-1065) basis set and the ECP28MDF effective core potential (Peterson et al., *J. Phys. Chem. A* **2006**, *110*, 13877-13883) for I and Zr^{IV}. All basis sets were obtained from the basis set exchange database (https://bse.pnl.gov/bse/portal). The grid used for numerical integration in DFT was set to "ultrafine," i.e., a pruned grid of 99 radial shells and 590 angular points per shell. The natures of all stationary points were determined by calculation of analytic vibrational frequencies, which were also used to compute molecular partition functions (298 K, 1 atm) using the conventional particle-in-a-box, rigid-rotator, quantum mechanical harmonic oscillator approximation (Cramer, C. J. *Essentials of Computational Chemistry: Theories and Models, 2nd ed.*; John Wiley & Sons: Chichester, **2004**), except that all vibrational frequencies below 50 cm^{-1} were replaced with values of 50 cm^{-1} (the quasi-harmonic-oscillator approximation, (Cramer, C. J. *Essentials of Computational Chemistry: Theories and Models, 2nd ed.*; John Wiley & Sons: Chichester, **2004**). Zero-point vibrational energies and thermal contributions to enthalpy were determined from these partition functions. For transition-state structures, the presence of a single imaginary frequency corresponding to the reaction path of interest was confirmed.

Electronic energies were further refined by performing single point calculations with the M06-2X (Zhao et al., *Theor. Chem. Acc.* **2008**, 120, 215-241) meta-GGA hybrid density functional on gas phase optimized geometries with the larger Def2-TZVP (Weigend et al., *Phys. Chem. Chem. Phys.* **2006**, *8*, 1057-1065) basis set on all elements and ECP28MDF on I and Zr^{IV} atoms using the SMD continuum solvation model (Marenich et al., *J. Phys. Chem. B* **2009**, *113,* 6378-6396) with parameters for water (ε = 78.355). CM5 charges were also computed for all systems considered in this study at the M06-2X(SMD, water)/def2-TZVP|ECP28MDF//M06-L(gas)/Def2-SVP|ECP28MDF (Marenich et al., *J. Chem. Theory Comput.* **2012**, *8,* 527-541). Default convergence criteria for geometry optimizations and single point energy calculations were used. All reported extended and truncated cluster free energies and enthalpies are computed by combining M06-2X(SMD, water) single point energies with thermochemical contributions obtained at the M06-L(gas phase) level. All cluster computations for mechanistic studies were carried out with Gaussian 16 (Frisch et al., *Gaussian 16,* Gaussian, Inc.*:* Wallingford, CT, **2013**).

Table S2. Computed M06-L key bond distances of different DMNP bonded (transition states for water addition in parenthesis) UiO-66 MOFs as well as M062X(SMD) CM5 charges (X = Br and I; see Figure S28 and Figure 5 of the main text for structures and atom labeling).

	***ortho*-UiO-66-I**	**alter-UiO-66-I**	***meta*-UiO-66-I**	***ortho*-UiO-66-Br**	**UiO-66-H**
$\Delta G^{\ddagger}$	11.0	12.2	19.5	13.7	19.9
X–O(Me)	3.405 (3.267)	3.398 (3.277)	5.829 (5.767)	3.550 (3.469)	-
X–O(P)	3.882 (3.651)	3.887 (3.713)	6.615 (6.702)	4.678 (3.458)	-
Q_{X}	0.028 (0.013)	0.029 (0.025)	-0.004 (-0.004)	-0.002 (0.013)	-
$Q_{O(Me)}$	-0.250 (-0.274)	-0.249 (-0.274)	-0.234 (-0.272)	-0.235 (-0.273)	-0.235 (-0.277)

$Q_{O(P)}$	-0.380 (-0.424)	-0.381 (-0.422)	-0.386 (-0.425)	-0.386 (-0.425)	-0.390 (-0.431)

NMR Spectroscopy

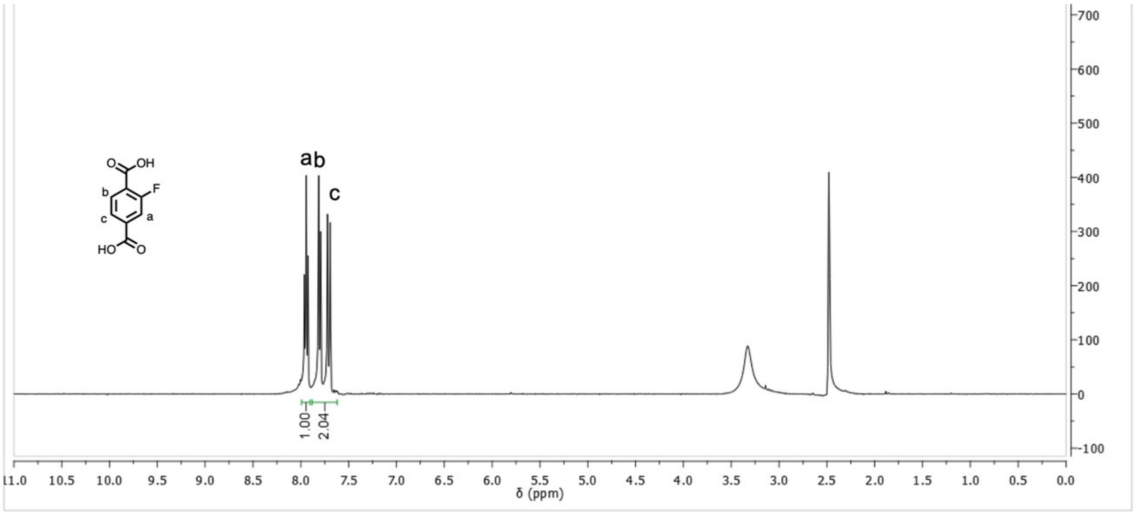

Figure S1. ^{1}H NMR of 2-fluoroterephthalic acid.

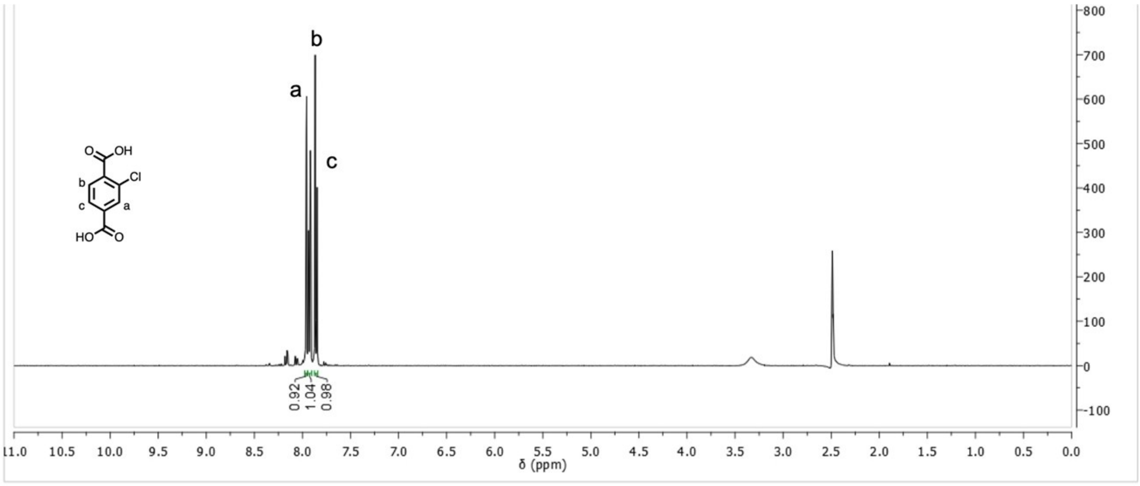

Figure S2. ^{1}H NMR of 2-chloroterephthalic acid.

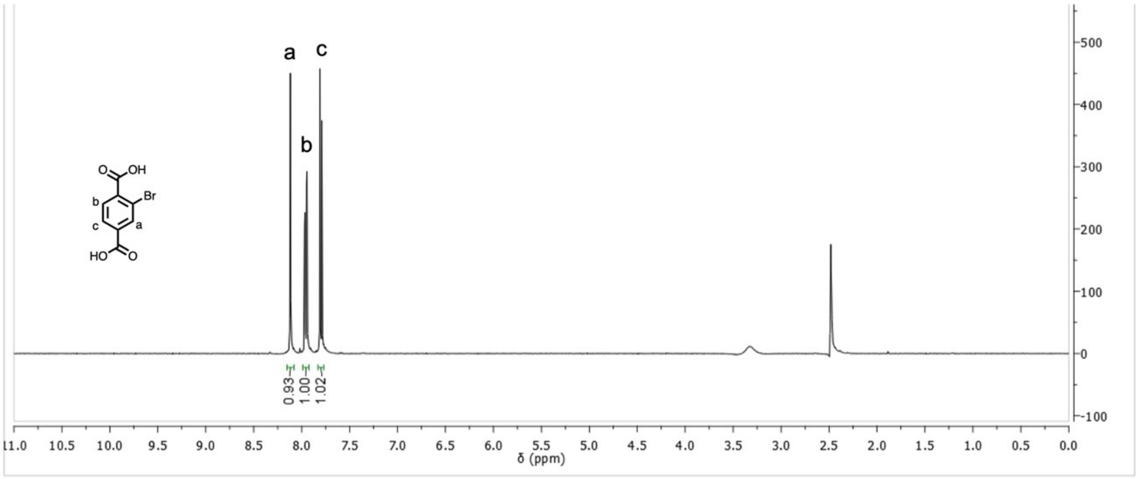

Figure S3. ^{1}H NMR of 2-bromoterephthalic acid.

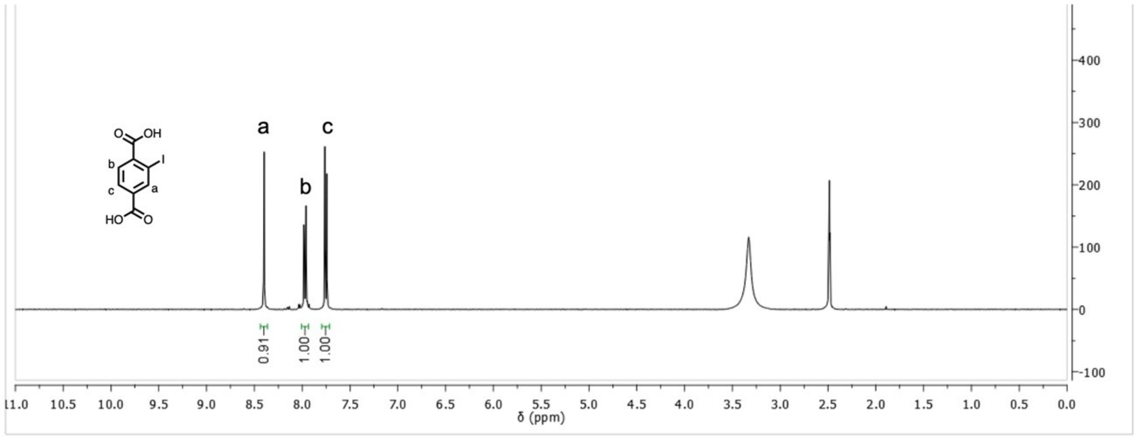

Figure S4. ^{1}H NMR of 2-iodoterephthalic acid.

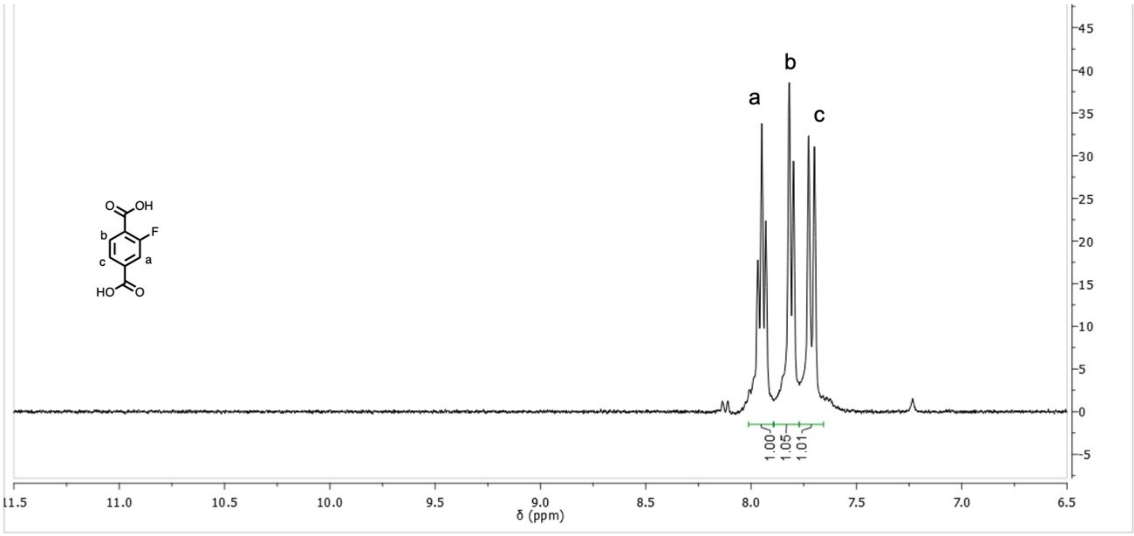

Figure S5. ^{1}H NMR analysis of digested UiO-66-F.

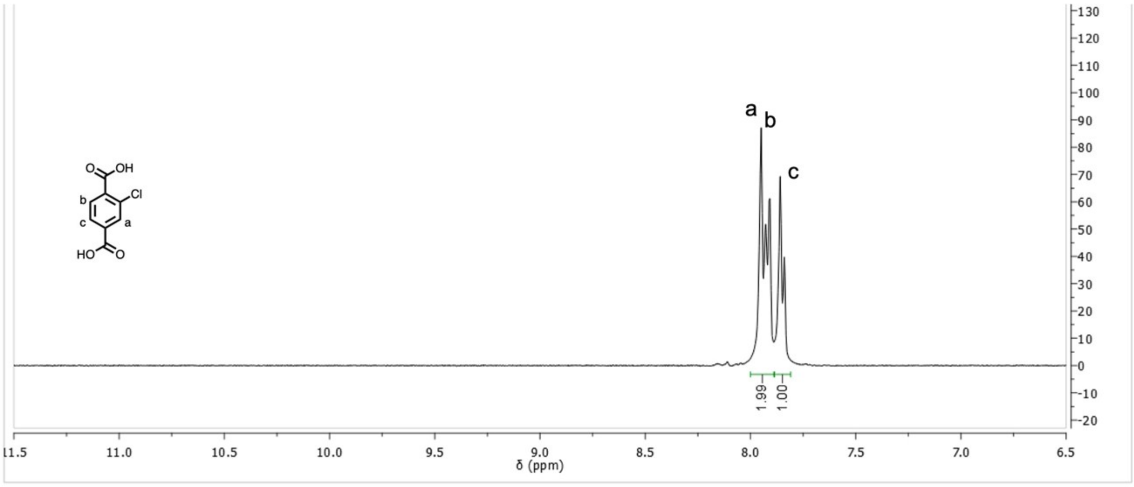

Figure S6. ^{1}H NMR analysis of digested UiO-66-Cl.

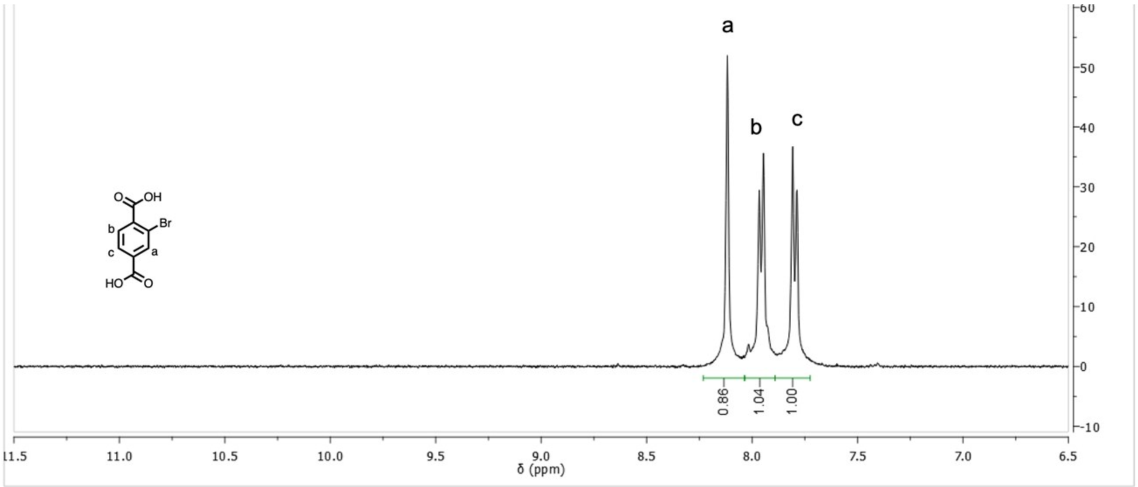

Figure S7. ^{1}H NMR analysis of digested UiO-66-Br.

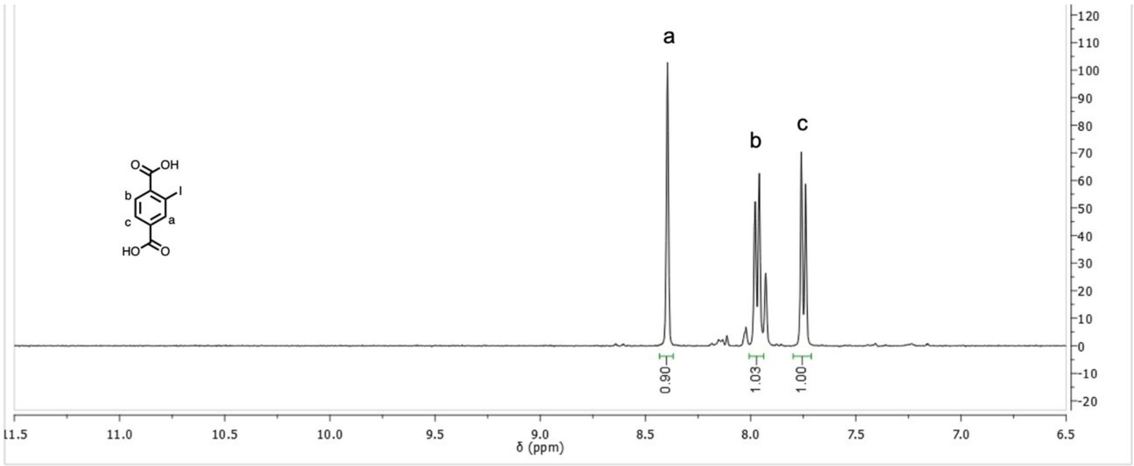

Figure S8. ^{1}H NMR analysis of digested UiO-66-I.

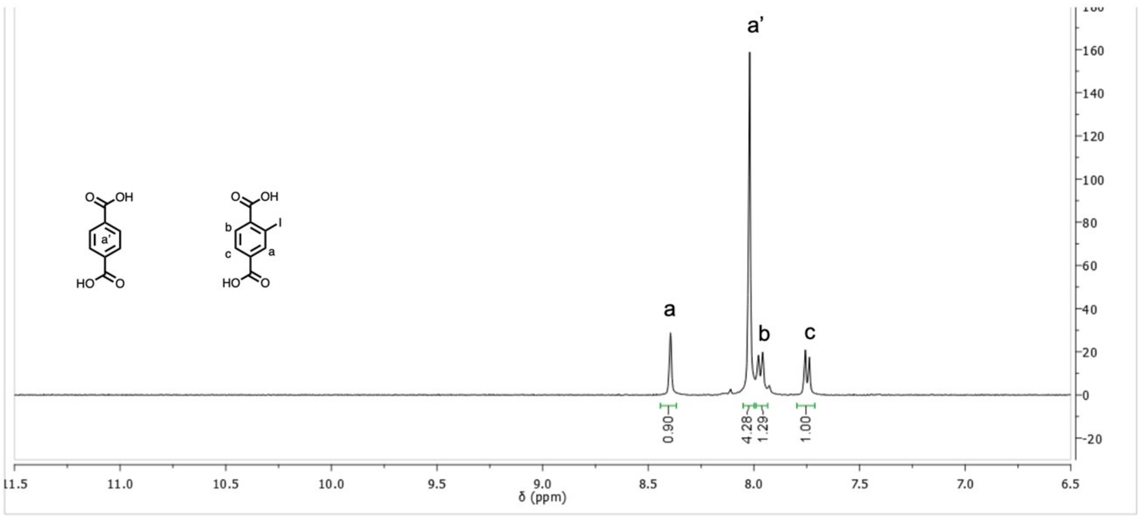

Figure S9. ^{1}H NMR analysis of digested UiO-66-I$_{50\%}$.

Scanning Electron Microscopy (SEM)

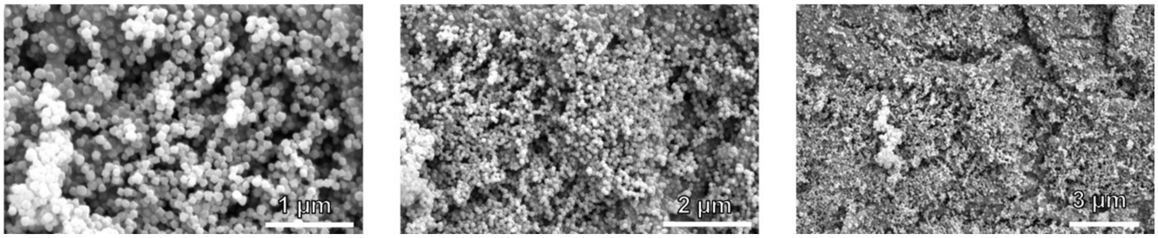

Figure S10. SEM images of UiO-66.

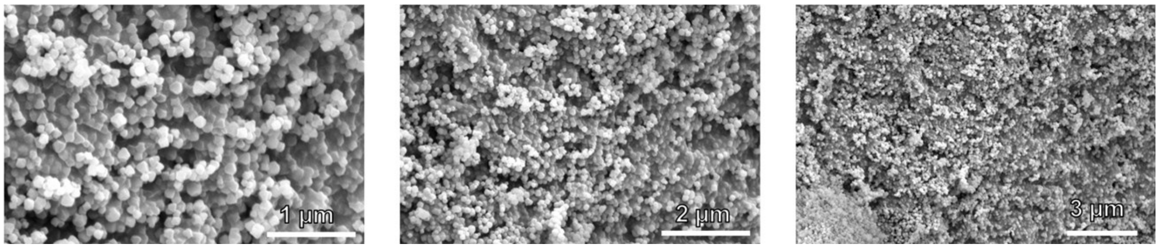

Figure S11. SEM images of UiO-66-F.

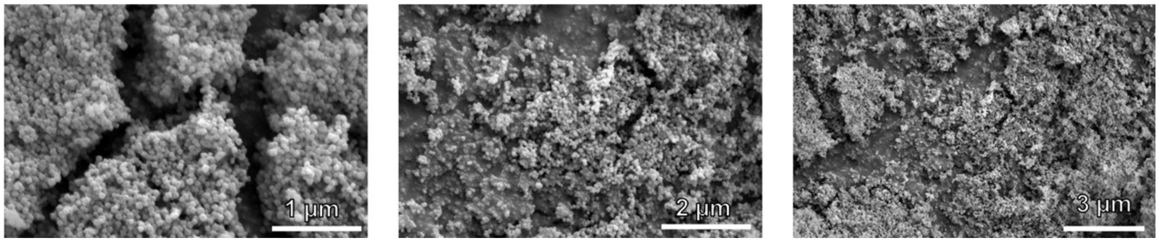

Figure S12. SEM images of UiO-66-Cl.

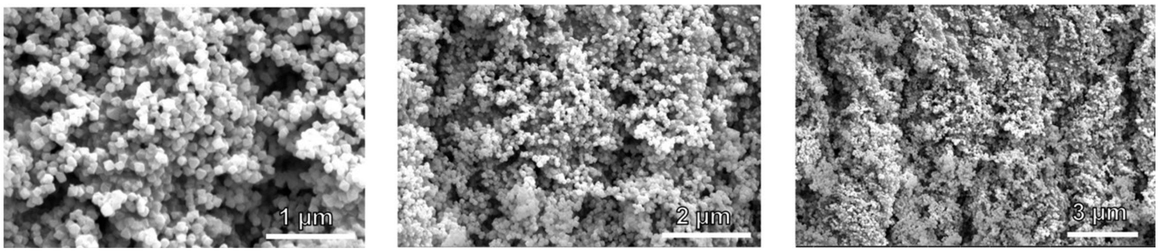

Figure S13. SEM images of UiO-66-Br.

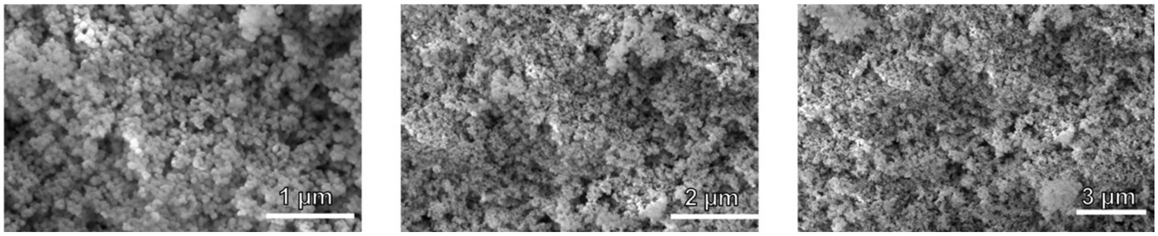

Figure S14. SEM images of UiO-66-I.

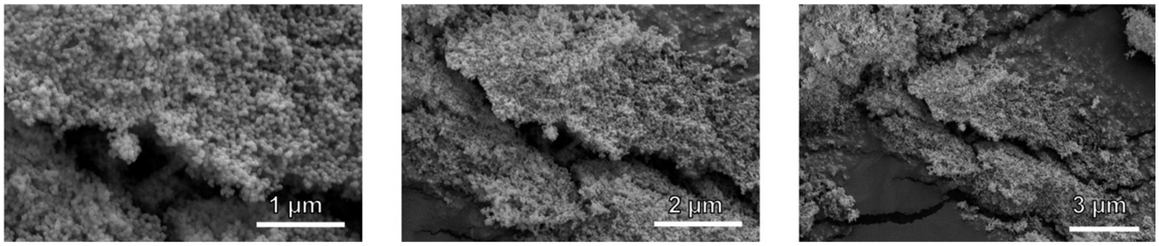

Figure S15. SEM images of mixed ligand UiO-66-I$_{50\%}$.

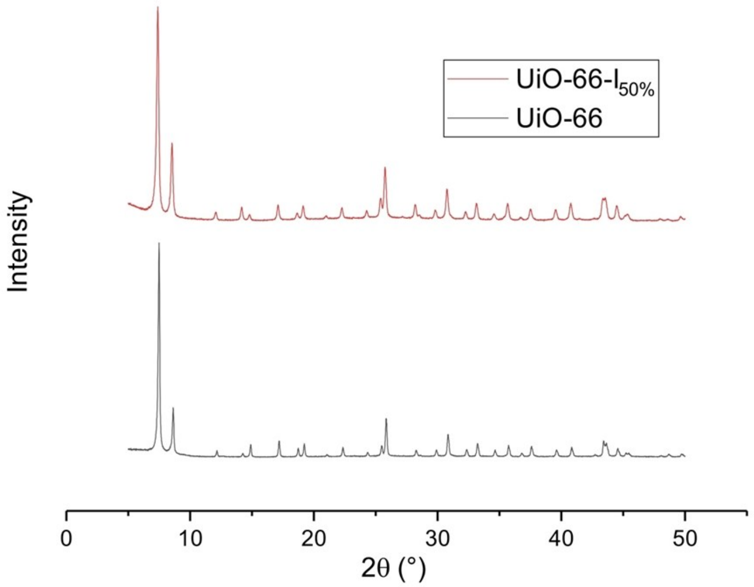

Figure S16. PXRD of mixed ligand UiO-66-I$_{50\%}$.

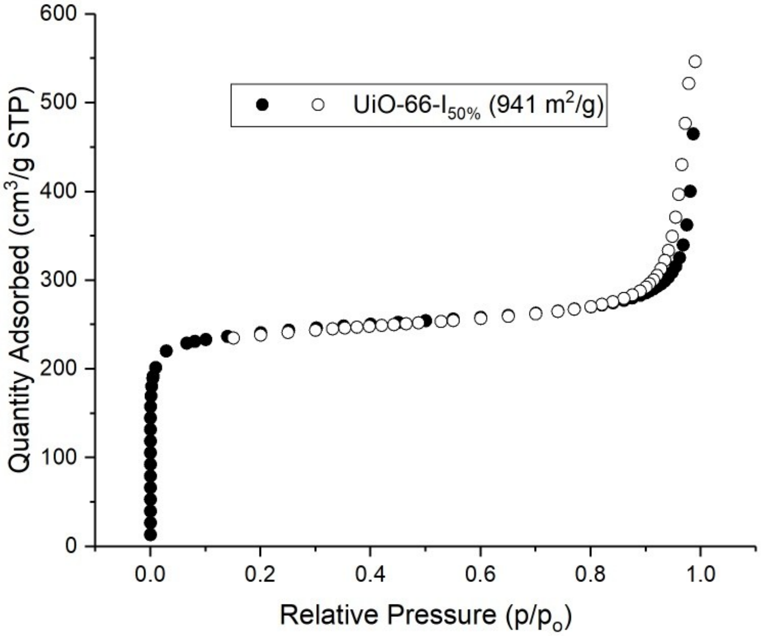

Figure S17. N_2 sorption isotherm of mixed ligand UiO-66-I$_{50\%}$.

Thermogravimetric Analysis (TGA)

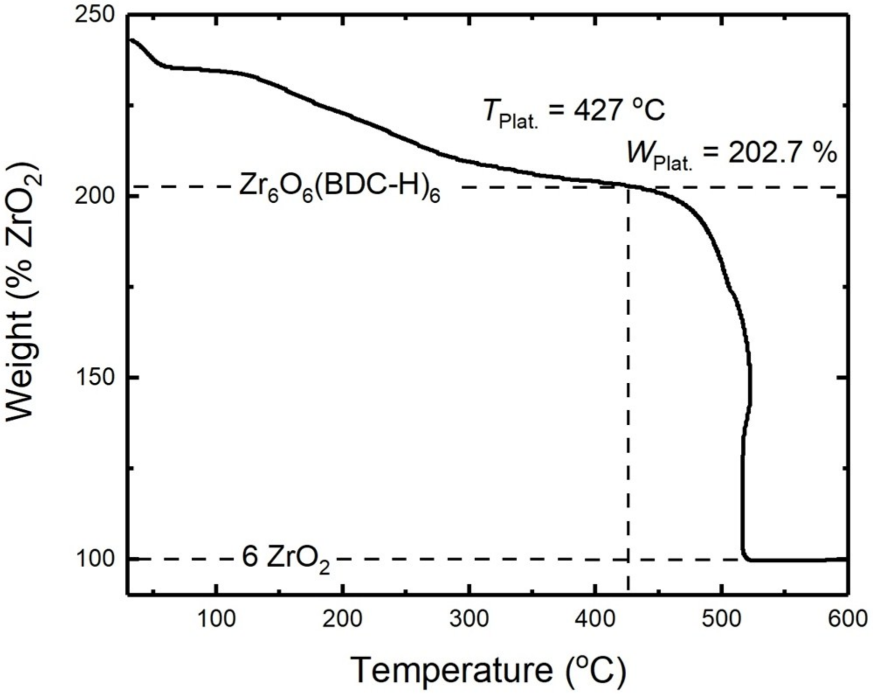

Figure S18. TGA trace for UiO-66.

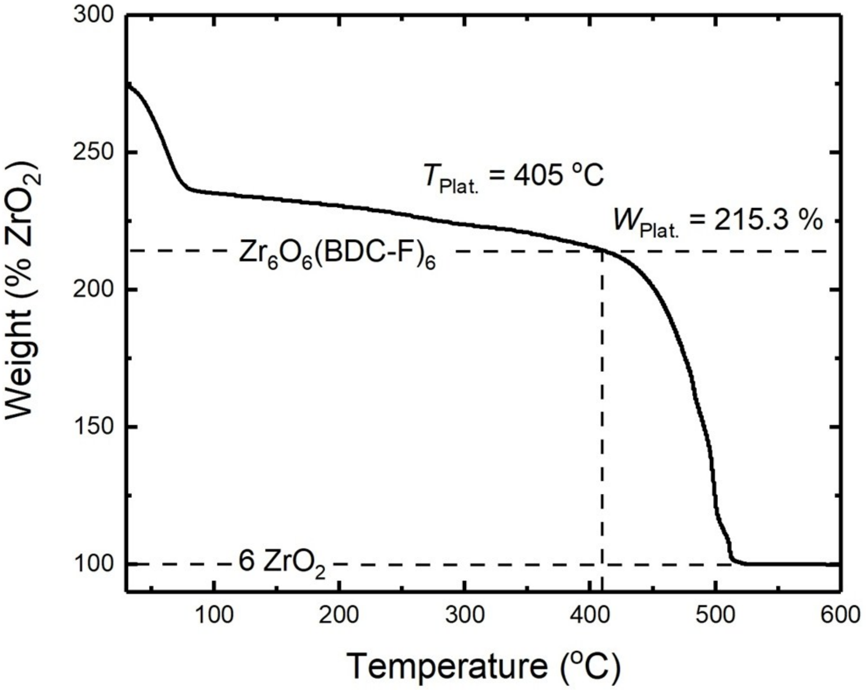

Figure S19. TGA trace for UiO-66-F.

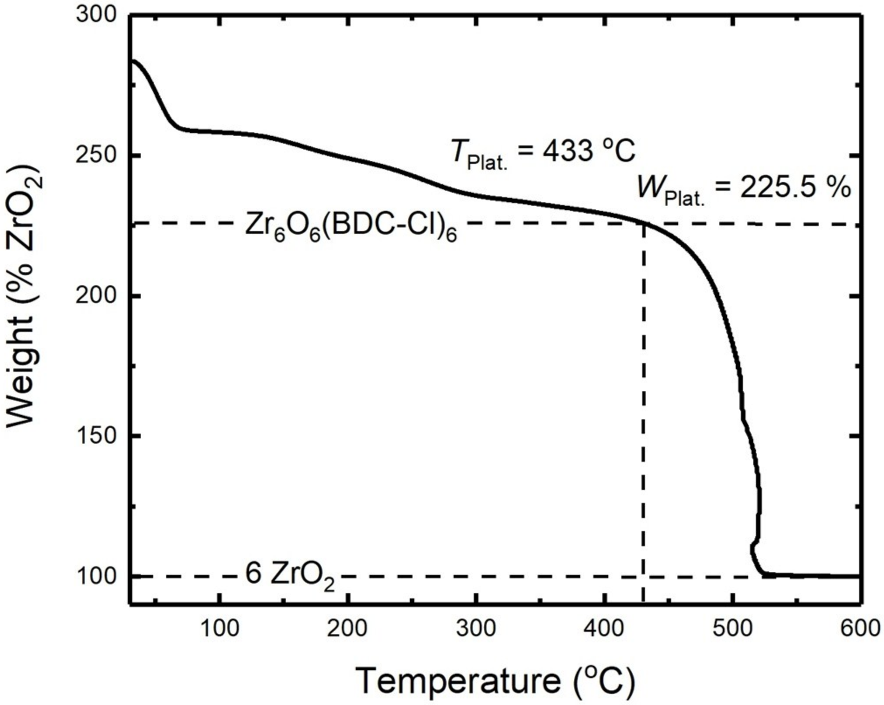

Figure S20. TGA trace for UiO-66-Cl.

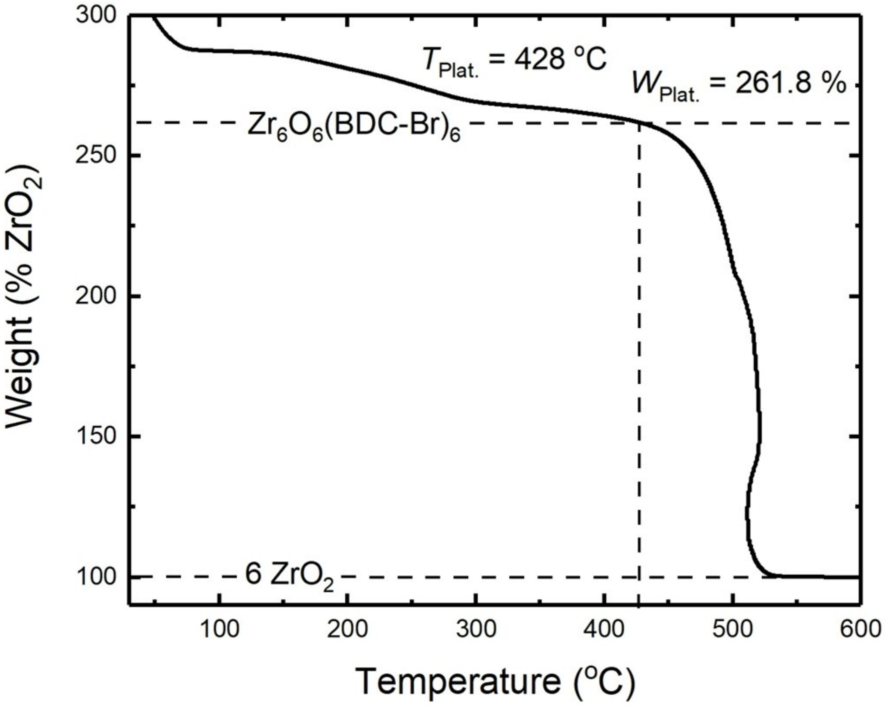

Figure S21. TGA trace for UiO-66-Br.

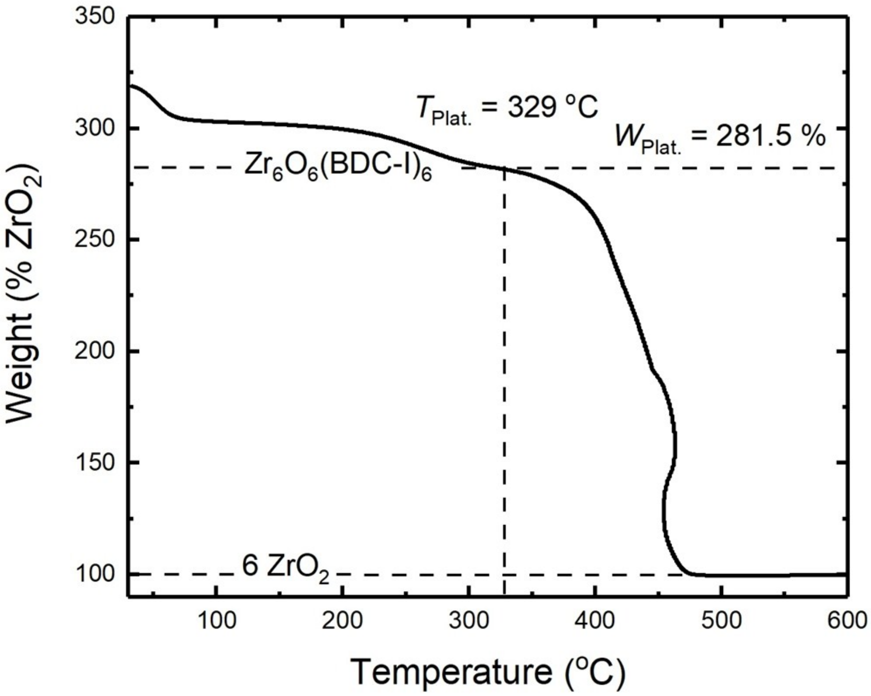

Figure S22. TGA trace for UiO-66-I.

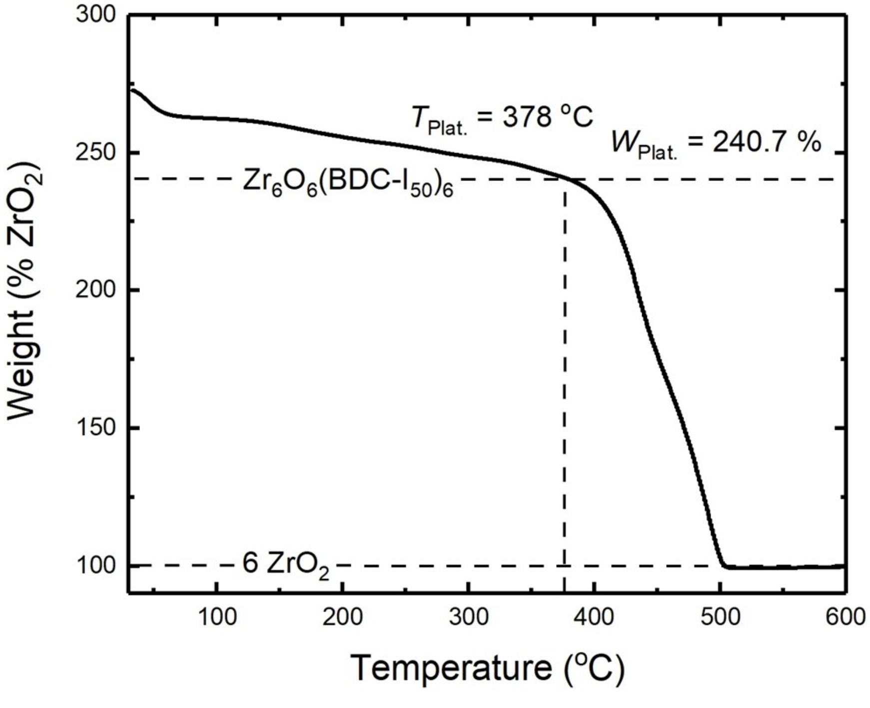

Figure S23. TGA trace for UiO-66-$I_{50\%}$.

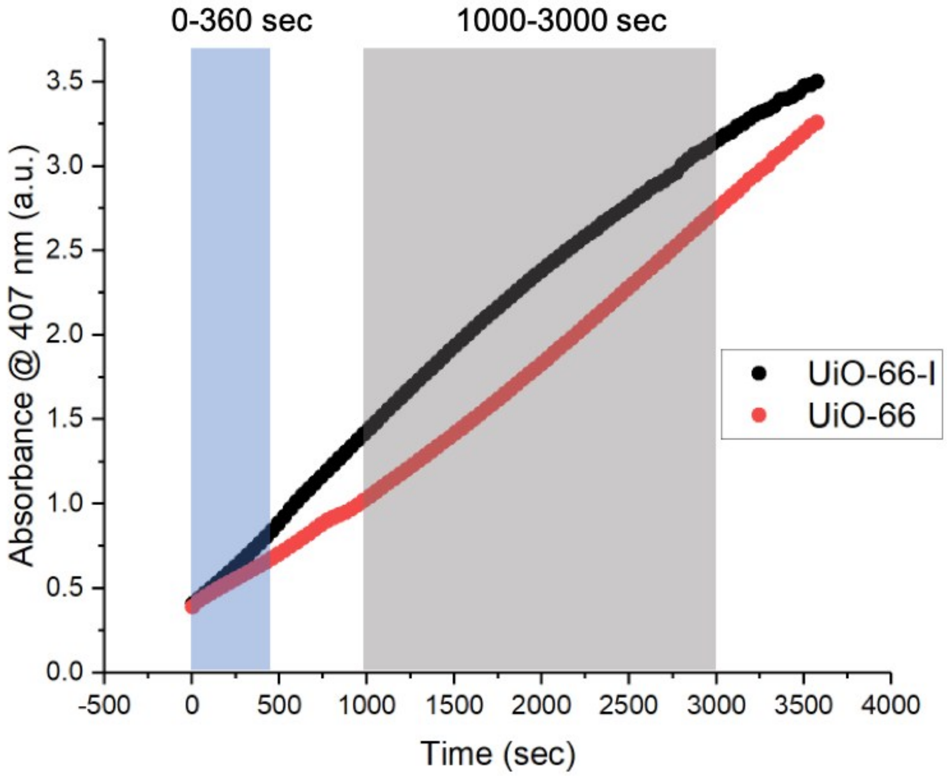

Figure S24. Absorbance (407 nm) vs. time (sec) monitoring the conversion of DMNP to *p*-nitrophenol for UiO-66 and UiO-66-I. This chart highlights the change in slope in the rate of conversion after the 500 sec point for UiO-66-I.

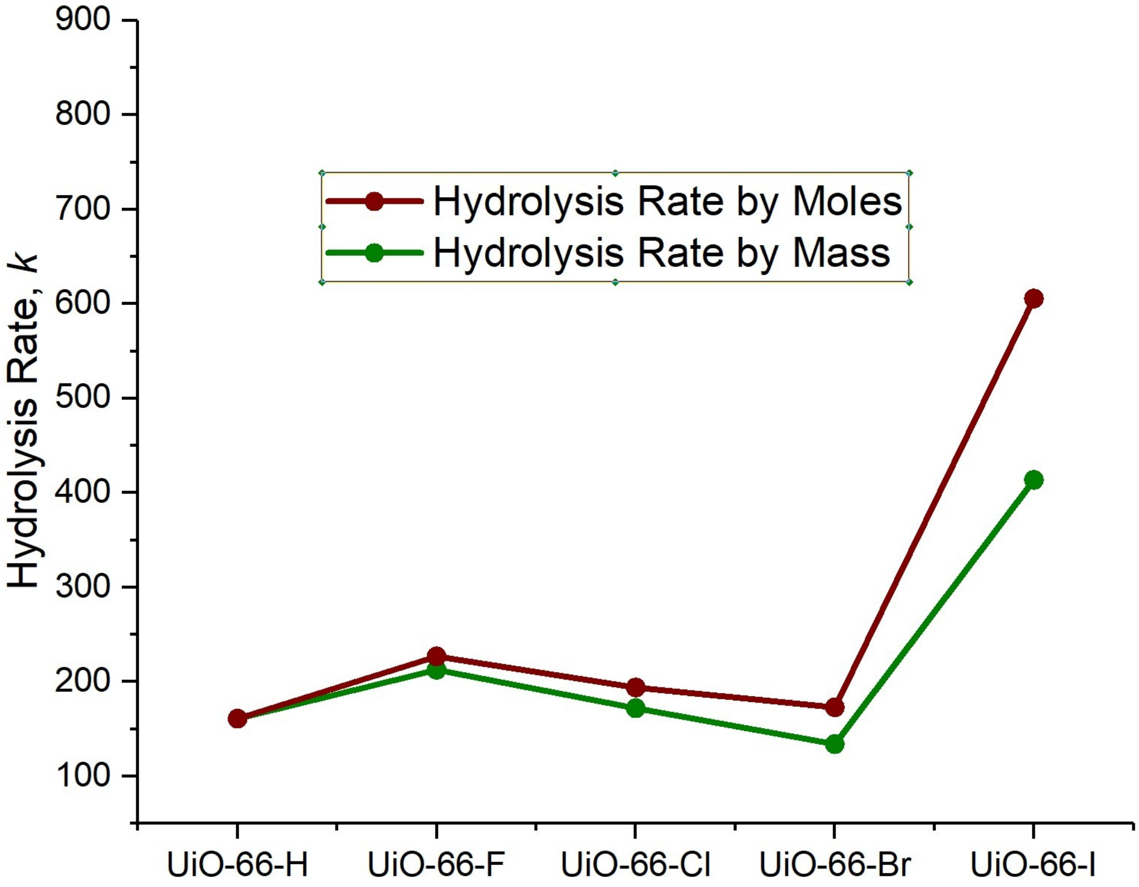

Figure S25. DMNP hydrolysis rate of the MOFs in this study by mass vs. mole generated after applying the correction factor (vide infra).

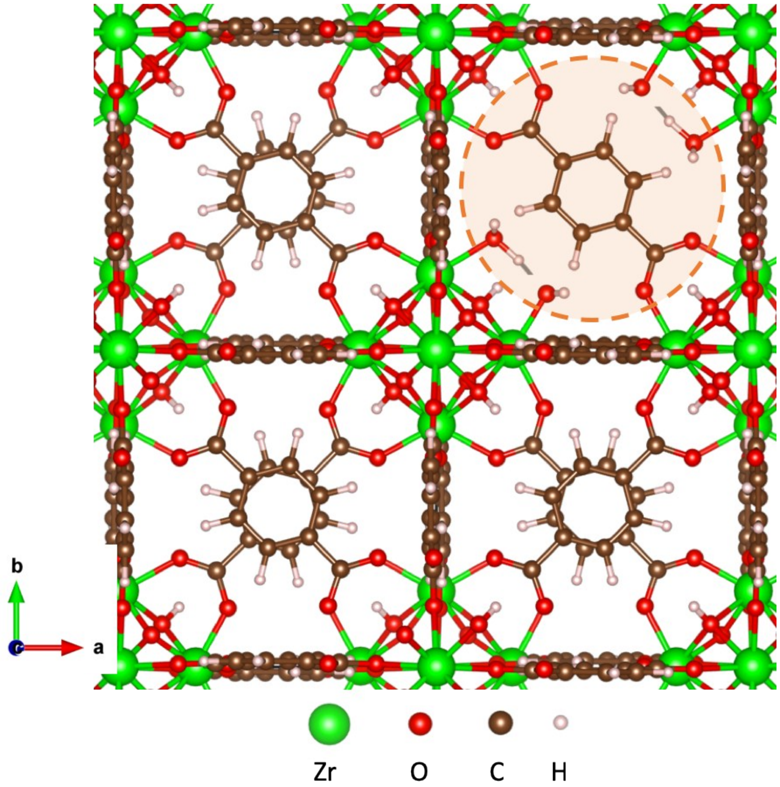

Figure S26. PBE-D3/DZVP-MOLOPT optimized crystal structure of the mono-defective UiO-66 (i.e. with 11 BDC linkers). Generated empty pore after the BDC linker removal is highlighted.

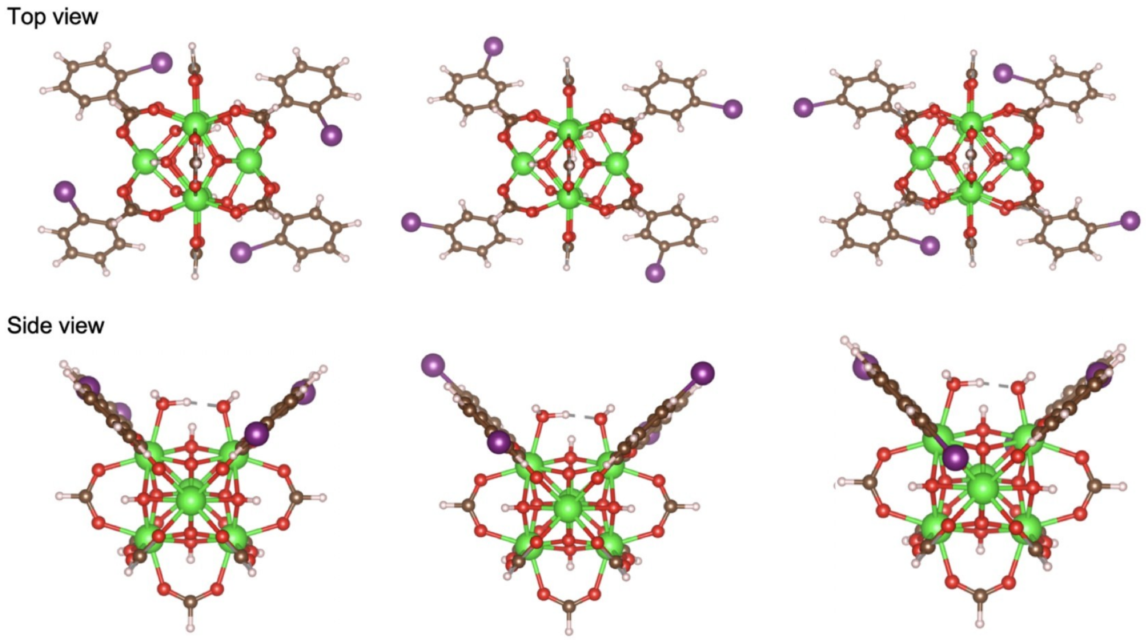

Figure S27. Top view and side view of the M06-L(gas)/Def2-SVP|ECP28MDF optimized mono-defective *ortho* (left), *meta* (middle) and alternated *ortho* and *meta* (right) iodine functionalized UiO-66 MOFs.

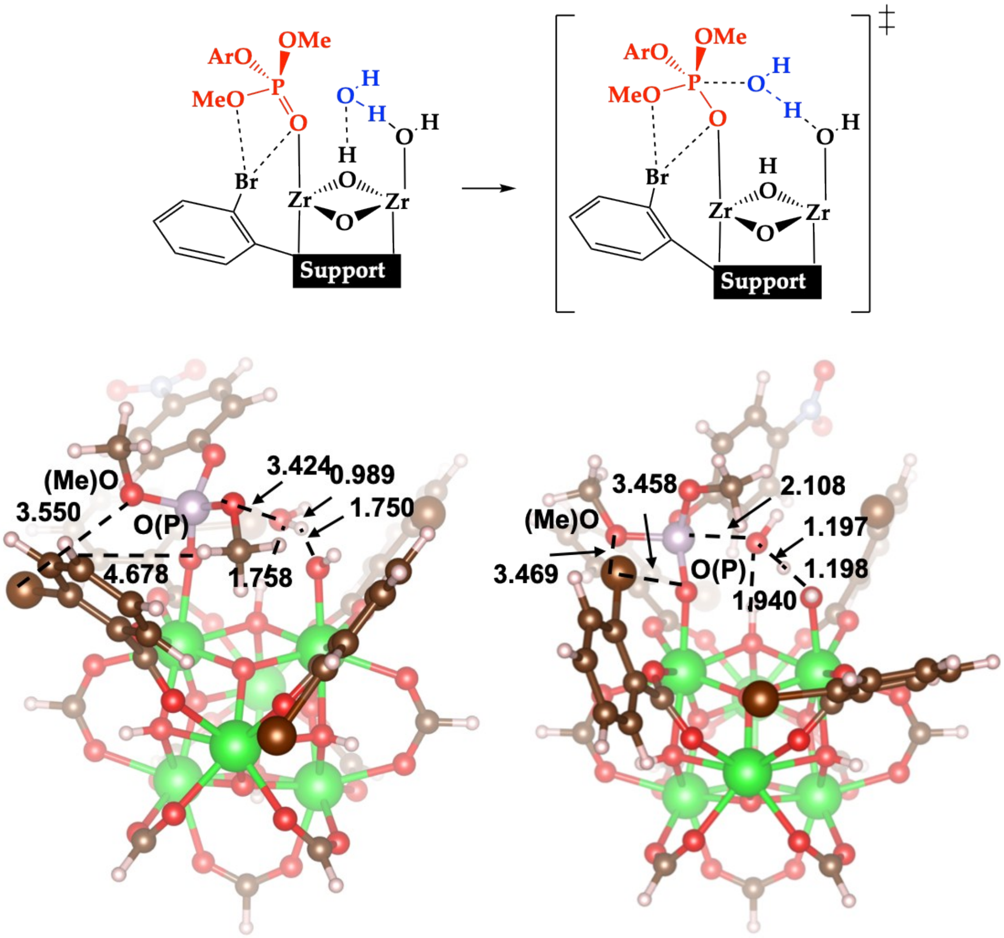

Figure S28. M06-L computed key bond lengths (Å) in *ortho*-UiO-66-Br cluster models of DMNP bonded (left) and transition state for nucleophilic attack of water to the P center (right) (ArO = 4-nitrophenoxide). Gray, white, red, blue, light purple, dark purple and green represent C, H, O, N, P, I, and Zr atoms, respectively.